

# Preliminary chemical reduction for synthesizing a stable porous molecular conductor with neutral metal nodes

Shohei Koyama<sup>1</sup>, Tappei Tanabe<sup>1</sup>, Shinya Takaishi<sup>1</sup>, Masahiro Yamashita<sup>1,2</sup> and Hiroaki Iguchi\*<sup>1</sup>

<sup>1</sup>Department of Chemistry, Graduate School of Science, Tohoku University, 6-3  
Aramaki-Aza-Aoba, Aoba-ku, Sendai, Miyagi 980-8578, Japan

<sup>2</sup>School of Materials Science and Engineering, Nankai University, Tianjin 300350, China

## Table of Contents

Experimental details	S2
Crystallographic data of <b>PMC-2</b> (Table S1)	S5
Crystallographic data of <b>2'</b> (Table S2)	S6
Crystal structure of <b>2'</b> (Fig. S1)	S7
Crystal structure of <b>PMC-2</b> with DMA molecules (Fig. S2)	S8
Solvent-accessible voids in <b>PMC-2</b> and <b>PMC-1</b> (Fig. S3)	S9
Calculated LUMO of NDI-py and NDI-py dimer (Fig. S4)	S11
Solid-state cyclic voltammetry of <b>PMC-2</b> (Fig. S5)	S12
Electron spin resonance spectrum of <b>PMC-2</b> (Fig. S6)	S13
Direct current (DC) magnetic susceptibility of <b>PMC-2</b> (Fig. S7)	S14
Thermogravimetry of <b>PMC-2</b> (Fig. S8)	S15
Weight loss of <b>PMC-2</b> under N <sub>2</sub> gas flow (Fig. S9)	S16
Time-dependent powder X-ray diffraction patterns of <b>PMC-2</b> (Fig. S10)	S16
Arrhenius plots of conductivities in <b>PMC-2</b> and <b>PMC-1</b> (Fig. S11)	S17
References	S17

## **Experimental details**

### **General experimental information**

All chemicals were used without further purification. Thermogravimetry (TG) analysis was performed on a SHIMADZU DTG-60H at a heating rate of 5 °C/min under a constant nitrogen flow (0.1 L/min). Powder X-ray diffraction (PXRD) patterns were collected on a Bruker D2 PHASER with Cu K $\alpha$  radiation ( $\lambda = 1.5406 \text{ \AA}$ ) at RT. IR spectra were recorded as KBr pellets on a JASCO FT/IR-4200 spectrometer at RT. UV-Vis-NIR absorption spectra were measured as KBr pellets on a JASCO V-670 spectrophotometer at RT. For acquiring IR and UV-Vis-NIR spectra under inert atmosphere, the KBr pellets were fabricated in glove box (MBRAUN UNILAB1200/780) filled with Ar gas, and then the pellets were set into a specially designed sealed optical cell individually.  $^1\text{H}$  NMR measurements were performed on Bruker AV500 at RT. The ESR spectrum was acquired by using a JEOL JES-FA100. The temperature dependence of the electrical conductivity was measured in a liquid He cryostat of a Quantum Design Physical Property Measuring System (PPMS) MODEL 6000 by using the two-probe method in direct current (DC) mode with Keithley sourcemeter model 2611. The resistance of the sample was measured under the application of a constant voltage (1 V). The cooling rate was 1K/min. The electrical leads (15  $\mu\text{m}\phi$  gold wires) were attached to a single crystal with carbon paste (Dotite XC-12 in diethyl succinate).

### **Syntheses**

Synthesis of *N,N'*-bis(4-pyridyl)-naphthalenediimide (NDI-py)

Naphthalene-1,4,5,8-tetracarboxylic dianhydride 3.2 g (0.012 mol) and 4-aminopyridine 2.5 g (0.026 mol) in 20 mL *N,N*-dimethylformamide (DMF) were stirred at 180 °C overnight. After cooled to RT, precipitated solid was filtered and recrystallized by DMF. Pale brown crystals were washed by MeOH carefully, then dried in desiccator (1.68 g, 33.0%).  $^1\text{H}$  NMR(500 MHz, 297 K, DMSO-*d*<sub>6</sub>)  $\delta$ : 8.80–8.84 (dd, 4H), 8.74–8.78 (s, 4H), 7.57–7.60 (dd, 4H). Anal. Calc. for C<sub>24</sub>H<sub>12</sub>N<sub>4</sub>O<sub>4</sub>: C, 68.57; H, 2.88; N, 13.33. Found: C, 68.43; H, 2.84; N, 13.48.

Synthesis of [Co(acac)<sub>2</sub>(MeOH)<sub>2</sub>]

10 mL H<sub>2</sub>O solution containing 2.58 g (0.020 mol) of CoCl<sub>2</sub> and 3.94 g (0.048 mol) of sodium acetate was mixed with 4.80 g (0.048 mol) of acetylacetone dissolved in 5 mL MeOH. Pale red solid was filtered and recrystallized by methanol to obtain red crystals (1.30 g, 20.3%). Anal. Calc. for C<sub>12</sub>H<sub>22</sub>CoO<sub>6</sub>: C, 44.87; H, 6.90; N, 0.00. Found: C, 44.75; H, 6.91; N, 0.00.

### Synthesis of RbBPh<sub>4</sub>

2.0 g (6.0 mmol) of sodium tetraphenylborate was dissolved into 10 mL H<sub>2</sub>O and mixed with 2 mL H<sub>2</sub>O solution containing 0.80 g (3.46 mmol) rubidium carbonate. White precipitate was filtered and dried in desiccator (2.37 g 97.8%). <sup>1</sup>H NMR(500 MHz, 297 K, DMSO-d<sub>6</sub>)  $\delta$ : 6.76–6.82 (t, 4H), 6.90–6.95 (t, 8H), 7.15–7.20 (m, 8H). Anal. Calc. for C<sub>24</sub>H<sub>20</sub>BRb: C, 71.32; H, 4.98; N, 0.00. Found: C, 71.32; H, 5.04; N, 0.00

### Synthesis of Rb<sub>0.5</sub>[Co(acac)<sub>2</sub>(NDI-py)]·2DMA (**PMC-2**)

**PMC-2** was synthesized by liquid-liquid diffusion method. 1 mL DMA solution containing 1.7 mg (4.0  $\mu$ mol) of NDI-py and 0.8 mg (4  $\mu$ mol) of cobaltocene was slowly layered on 1 mL DMA/CH<sub>2</sub>Cl<sub>2</sub> (95/5, v/v) solution containing 1.9 mg (5.9  $\mu$ mol) of [Co(acac)<sub>2</sub>(MeOH)<sub>2</sub>] and 2.1 mg (5.2  $\mu$ mol) of RbBPh<sub>4</sub>. Two weeks later, black rod-like single crystals were obtained (2.5 mg 69.9%). Anal. Calc. for C<sub>42</sub>H<sub>44</sub>CoN<sub>6</sub>O<sub>10</sub>Rb<sub>0.5</sub>: C, 56.40; H, 4.96; N, 9.40. Found: C, 55.21; H, 5.28; N, 9.54 Small quantities of [Co(acac)<sub>2</sub>(NDI-py)]·2DMA (**2'**) crystals were also obtained as impurities, which were removed by hands under a microscope before the characterization of **PMC-2**. Pure **2'** were obtained as brown block single crystals by the same synthetic procedure for **PMC-2** except no cobaltocene was used.

### Inductively coupled plasma (ICP) spectroscopy

Inductively coupled plasma (ICP) spectroscopy of metal levels was performed by using ThermoFisher, iCAP6500 at the Technical Division, School of Engineering, Tohoku University. **PMC-2** from two different batches were individually dissolved into 10% (v/v) H<sub>2</sub>SO<sub>4</sub> aqueous solution. The instrument was calibrated using 0, 0.2, 0.5, 1.0, 2.0, 5.0 parts per million (ppm) of standard calibration solutions with the same concentration of H<sub>2</sub>SO<sub>4</sub>. The emission intensity (at 238.8 nm for Co and at 780.0 nm for Rb) was measured three times and the average values were used to determine the concentration via calibration curve. Concentrations (ppm) in batch 1: Co, 3.049; Rb, 2.141, and in batch 2: Co, 4.080; Rb, 2.846. Therefore, the Rb/Co ratios were 0.4842 and 0.4810 for batch 1 and 2, respectively.

### Single-crystal X-ray structure determination

The diffraction data for **PMC-2** and **2'** were collected on a Rigaku Saturn 724+ CCD diffractometer equipped with graphite monochromated Mo K $\alpha$  radiation ( $\lambda = 0.7107 \text{ \AA}$ ). The crystal structure was solved using direct methods (SHELXT<sup>S1</sup>) and followed by Fourier synthesis. Structure refinement was performed using full matrix least-squares procedures with SHELXL<sup>S2</sup> on  $F^2$  in the Yadokari-XG 2009 software<sup>S3</sup> for **PMC-2** and in the Olex2 software.<sup>S4</sup> for **2'**.

### **Magnetic measurements**

Magnetic susceptibility measurements were performed on Quantum Design SQUID magnetometers MPMS-XL, PPMS VSM system. Direct current (DC) measurements were performed in the range of 1.8–300 K in DC magnetic field of 1000 Oe. Randomly oriented polycrystalline samples were used for the measurements. Diamagnetic contributions of sample and sample holder estimated by using Pascal's constants were carried out.

### **Computational methods**

Density functional theory (DFT) calculations were performed using a Gaussian 16 package. The B3LYP/6-31G(d) basis sets were used for the calculation of LUMO orbitals. The atomic coordination of NDI-py ligands was extracted from the cif files of **PMC-1** reported herein and used for the calculation without any optimizations. The molecular orbital energies were presented against the vacuum level standard. These results are shown in Fig. S4. Because the contribution of the pyridyl-N orbitals to the LUMO orbitals of the ligands are small, we ignored the changes in molecular orbitals derived from the coordination to metal ions. Quantum chemistry calculation in charge transfer properties was performed using density functional theory (DFT) methods employing the Amsterdam-density-functional (ADF 2019.03) program package. Transfer integral between NDI-py has been investigated by PW91/TZP methods without structural optimization.

### **Solid-state cyclic voltammetry**

The solid-state cyclic voltammetry measurements were carried out using a standard three-electrode cell with an ALS/CH Instruments Electrochemical Analyzer Model 620D. The working electrode was a glassy carbon (GC) electrode. Solid **PMC-2** was transferred to the surface of the GC electrode by the mechanical attachment method.<sup>S5</sup> Platinum and silver wires were used for counter and quasi-reference electrodes, respectively. The potential of the quasi-reference electrode was calibrated by using ferrocene (Fc) as an external standard. The cyclic voltammogram of **PMC-2** was acquired in dried acetonitrile under a nitrogen flow at scan rate of 100 mV/s

## Crystallographic data of PMC-2

Table S1 Crystallographic details for **PMC-2**

Radiation type, wave length	Mo K $\alpha$ , 0.71073 Å
Empirical formula	C <sub>42</sub> H <sub>44</sub> CoN <sub>6</sub> O <sub>10</sub> Rb <sub>0.5</sub>
Formula weight	894.49 g/mol
Crystal system	Hexagonal
Space group	<i>P</i> 6 <sub>4</sub> 22
Crystal size	0.20 × 0.03 × 0.03 mm <sup>3</sup>
Crystal color	Black
Crystal shape	Rod
Unit cell dimensions	<i>a</i> = 19.8453(7) Å <i>c</i> = 9.5591(7) Å
Volume	<i>V</i> = 3260.3(3) Å <sup>3</sup>
Temperature	120(2) K
<i>Z</i>	3
Density (calculated)	1.367 Mg/m <sup>3</sup>
Absorption coefficient	1.013 mm <sup>-1</sup>
<i>R</i> <sub>1</sub> , <i>wR</i> <sub>2</sub> [ <i>I</i> > 2 $\sigma$ ( <i>I</i> )]	0.0594, 0.1500
<i>R</i> <sub>1</sub> , <i>wR</i> <sub>2</sub> [all data]	0.0728, 0.1816
<i>F</i> (000)	1146
Goodness of fit on <i>F</i> <sup>2</sup>	1.063
Flack parameter	0.05(1)

## Crystallographic data of 2'

Table S2 Crystallographic details for 2'

Radiation type, wave length	Mo K $\alpha$ , 0.71073 Å
Empirical formula	CH <sub>44</sub> CoN <sub>6</sub> O <sub>10</sub>
Formula weight	851.76 g/mol
Crystal system	monoclinic
Space group	<i>P2</i> <sub>1</sub> / <i>n</i>
Crystal size	0.2 × 0.08 × 0.08 mm <sup>3</sup>
Crystal color	brown
Crystal shape	block
Unit cell dimensions	<i>a</i> = 10.2874(6) Å <i>b</i> = 19.8376(9) <i>c</i> = 11.0367(6) Å $\beta$ = 111.416(6) °
Volume	<i>V</i> = 2096.8(2) Å <sup>3</sup>
Temperature	100(2) K
<i>Z</i>	2
Density (calculated)	1.349 Mg/m <sup>3</sup>
Absorption coefficient	0.473 mm <sup>-1</sup>
<i>R</i> <sub>1</sub> , <i>wR</i> <sub>2</sub> [ <i>I</i> > 2 $\sigma$ ( <i>I</i> )]	0.0449, 0.1021
<i>R</i> <sub>1</sub> , <i>wR</i> <sub>2</sub> [all data]	0.0730, 0.1141
<i>F</i> (000)	890
Goodness of fit on <i>F</i> <sup>2</sup>	1.028

## Crystal structure of 2'

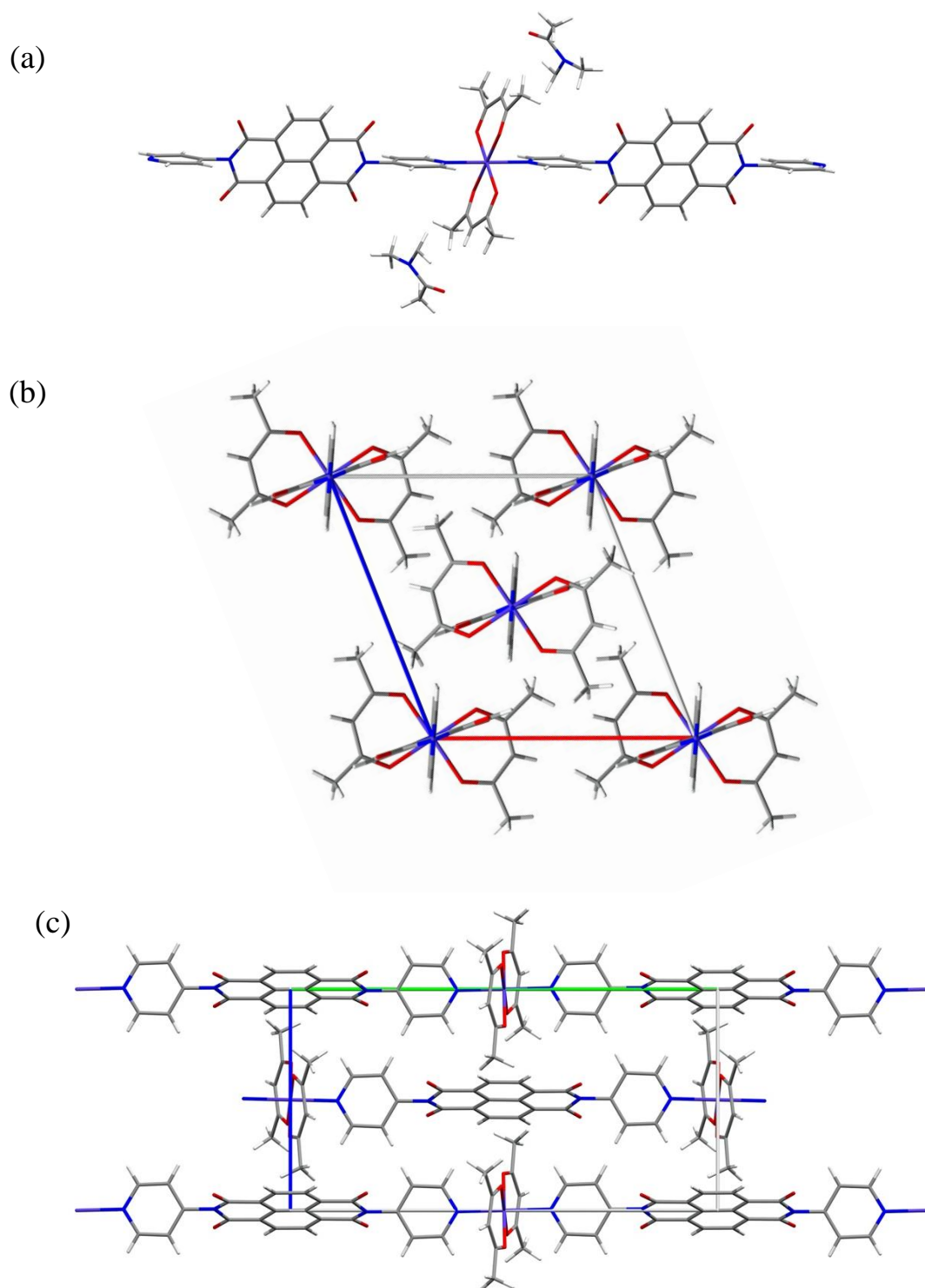


Fig. S1 Crystal structure of **2'**. (a) One dimensional coordination polymer in **2'**. Disorder of DMA molecule is omitted. (b,c) Packing structure of the coordination polymers viewed along (b) *b* axis and (c) *a* axis. DMA molecules are omitted for clarity. Purple, Co; Red, O; Blue, N; Gray, C; White, H.

## Crystal structure of PMC-2 with DMA molecules

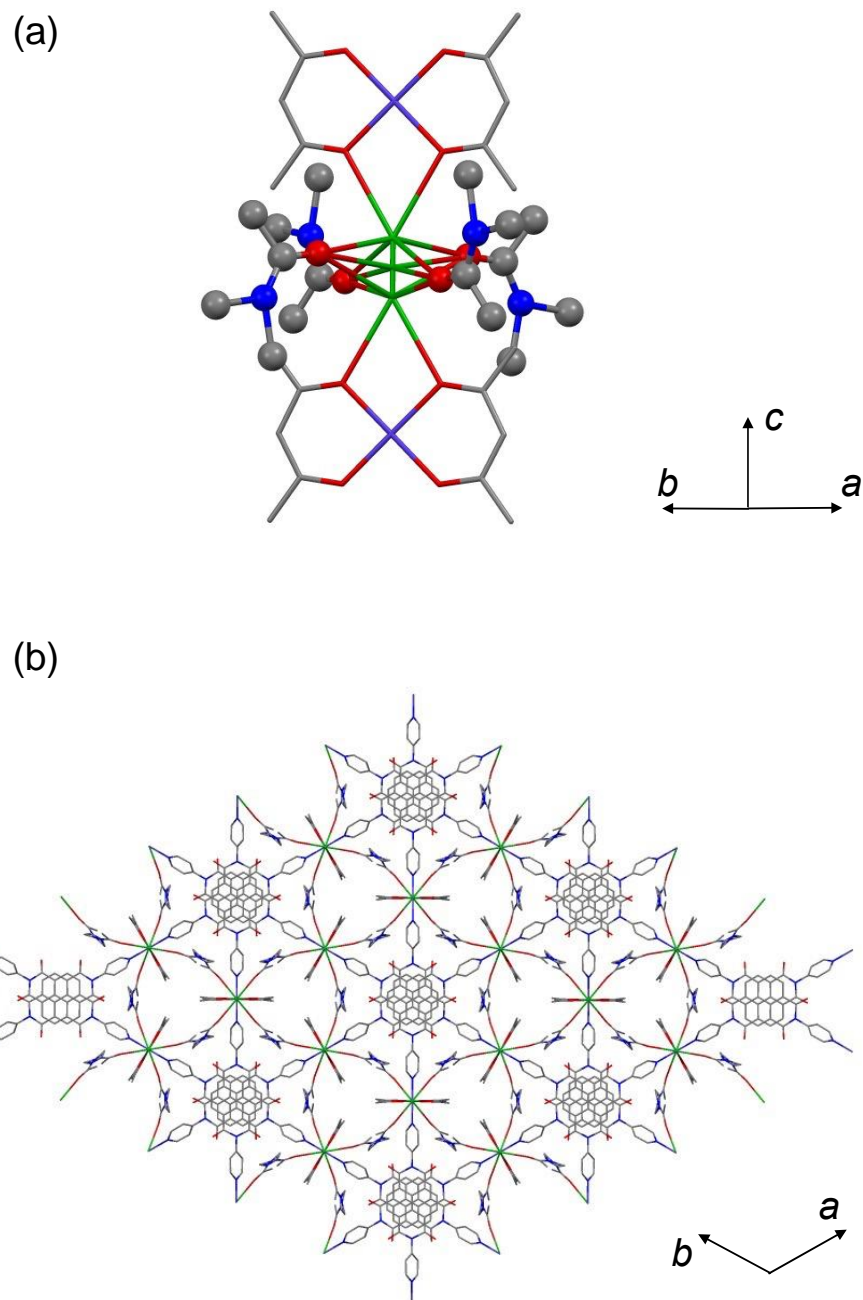


Fig. S2 Crystal structure of **PMC-2** with DMA molecules. (a) Coordination environment around  $\text{Rb}^+$  ion. (b) Perspective view along  $c$  axis. Occupancies of centred  $\text{Rb}^+$  ion (Rb1) and upper and lower  $\text{Rb}^+$  ions (Rb2) are 0.173 and 0.164, respectively. Thus the total occupancy of  $\text{Rb}^+$  ion is 0.5. The occupancy of each DMA molecule is also 0.5.

### Solvent-accessible voids in PMC-2 and PMC-1

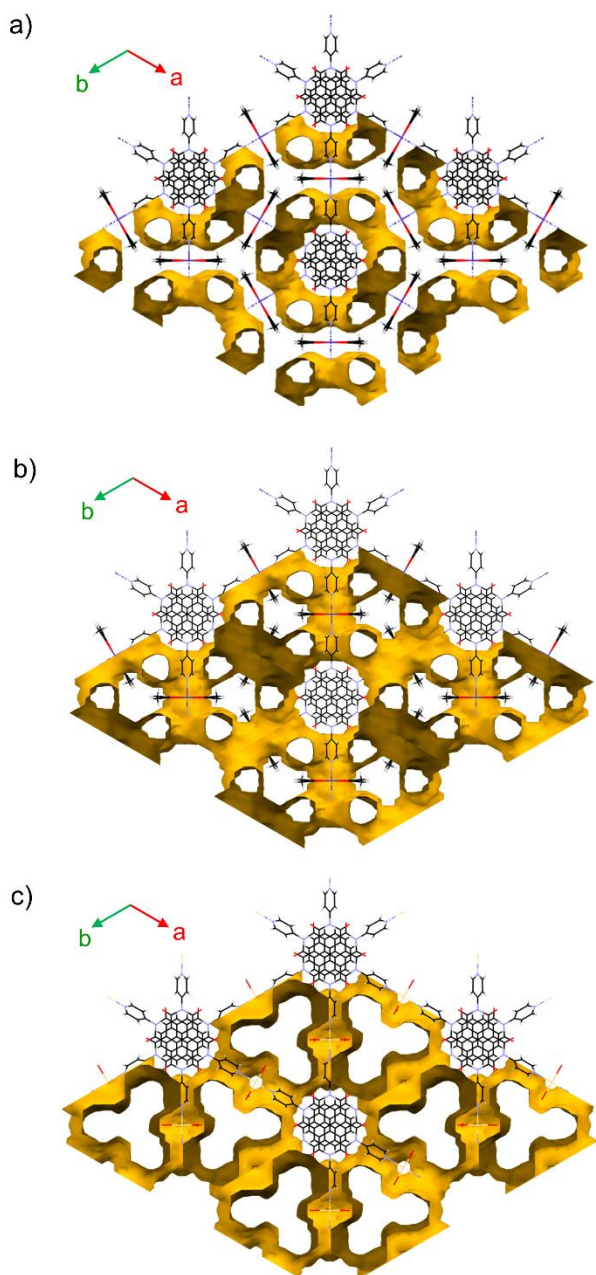


Fig. S3 Crystal structure with the representation of solvent-accessible voids of (a) **PMC-2**, (b) **PMC-2** without  $\text{Rb}^+$  ions and (c) **PMC-1**.

The solvent-accessible voids of **PMC-2** and **PMC-1** are depicted in Fig. S3. DMA molecules in the voids are omitted in Fig. S3a. Both DMA molecules and disordered  $\text{Rb}^+$  ions between  $[\text{Co}(\text{acac})_2]$  complexes are omitted in Fig. S3b. DMA molecules and nitrate ions in the voids were undetectable due to the dispersed electron density in Fig. S3c. The contact surface of the voids (brown) is drawn by a probe radius of  $1.5 \text{ \AA}$ . If the occupancy of  $\text{Rb}^+$  ions is 100% (Fig. S3a), the voids are isolated around  $\pi$ -stacked column to form donut-like 1D voids. On the other hand, if the occupancy of  $\text{Rb}^+$  ions is 0% (Fig. S3b), the donut-like voids are connected

each other via the space to which  $\text{Rb}^+$  ions are assigned. Since the actual occupancy of  $\text{Rb}^+$  ion is 50%, the voids in **PMC-2** should be the average of the above two cases and thus have 3D character. The voids in **PMC-1** is larger than those in **PMC-2** and have clear 3D character (Fig S3c). Apparently, a wide triangle 1D void in **PMC-1** is divided into three narrow 1D voids by  $[\text{Co}(\text{acac})_2]$  moieties in **PMC-2**.

## Calculated LUMO of NDI-py and NDI-py dimer

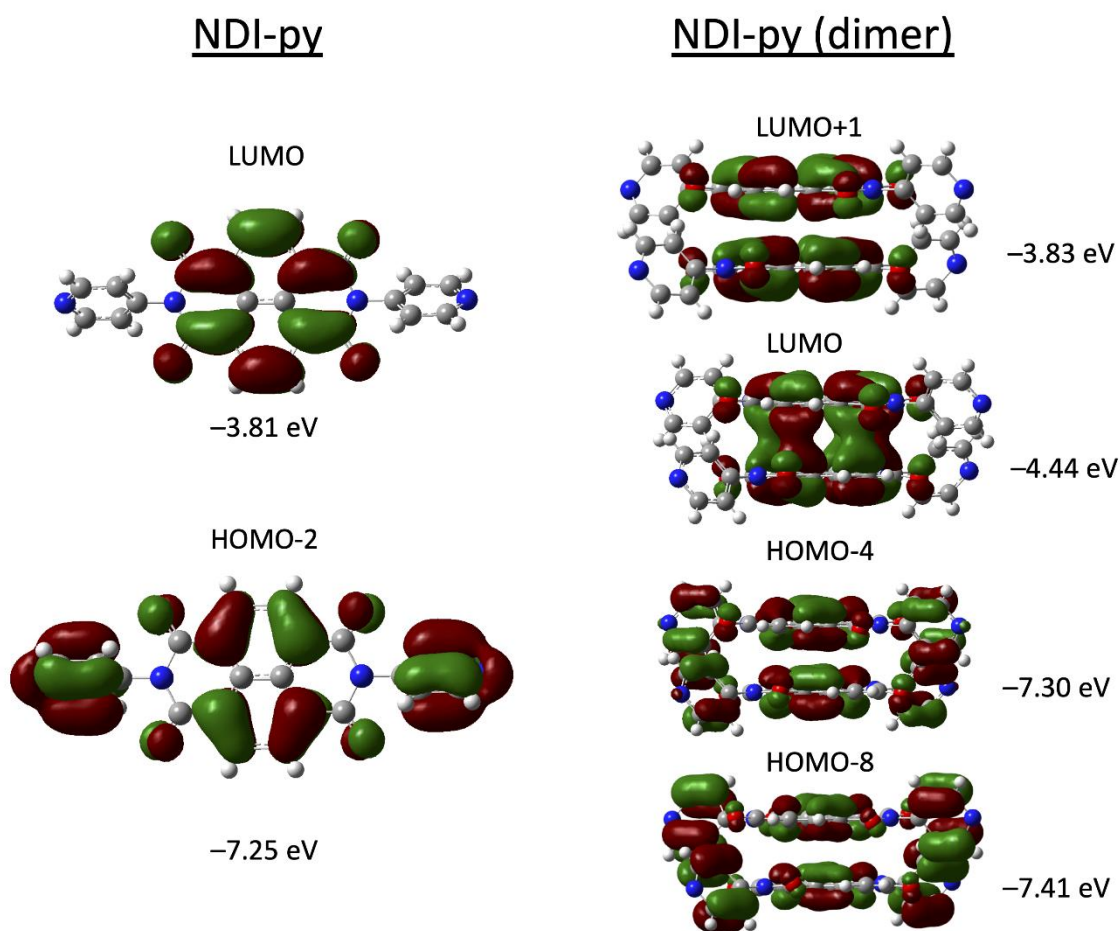


Fig. S4 Calculated LUMO of NDI-py and NDI-py(dimer)

The DFT calculations of the molecular orbitals were performed using the structure as it is from the crystal structure. Focusing on the molecular orbital of NDI-py (dimer), The LUMO is delocalized between the two  $\pi$ -conjugated planes, indicating that sufficient conjugation is occurring. As a result, the stabilization of LUMO (from  $-3.81$  eV to  $-4.44$  eV) is occurring. The conduction properties of **PMC-2** should be derived from the delocalization of radical electron along the infinite columnar structure.

### Solid-state cyclic voltammetry of PMC-2

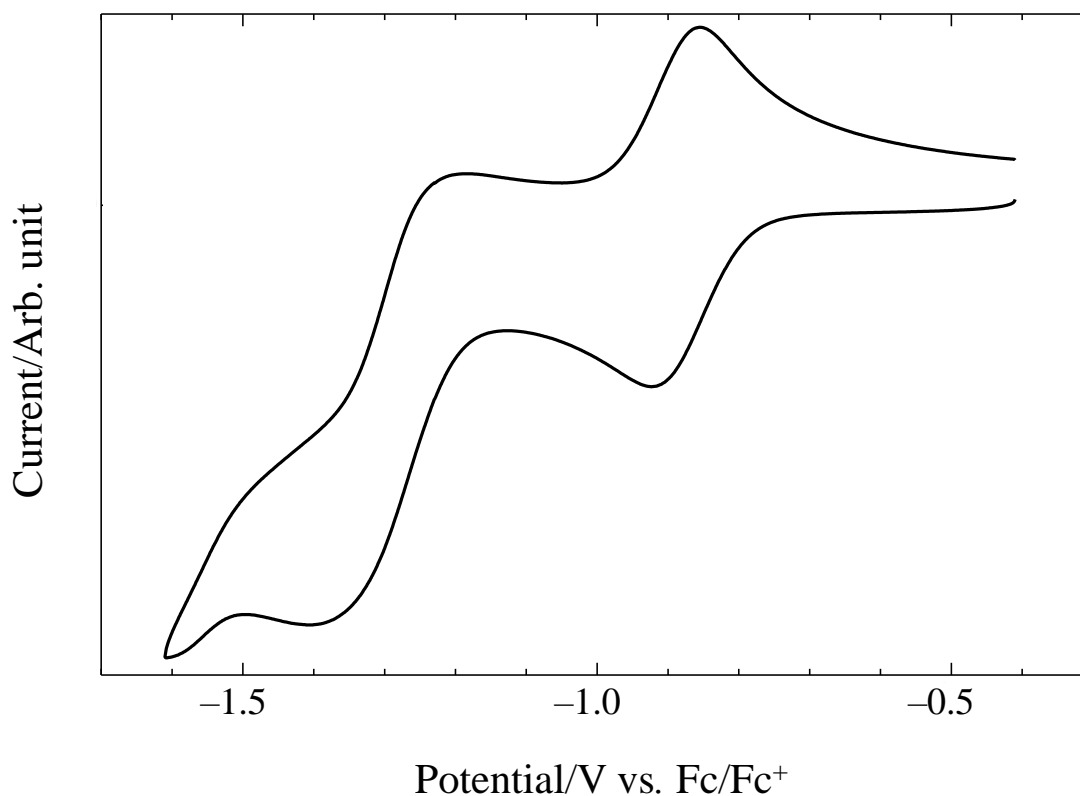


Fig. S5 Solid-state cyclic voltammogram of PMC-2

Solid-state cyclic voltammetry was recorded in 0.1 M TBAPF<sub>6</sub>/MeCN solution. **PMC-2** showed quasi-reversible redox wave at  $-0.889$  V vs Fc/Fc<sup>+</sup>. Considering that the redox potential of Fc/Fc<sup>+</sup> is  $-5.06$  eV with respect to the vacuum level, the potential of this redox wave is  $-4.17$  eV ( $E_{\text{LUMO}} = -5.06 \text{ eV} - (E_{1/2})$ ), which is corresponding to the LUMO of NDI-py dimer in the DFT calculation (Fig. S4).

## Electron spin resonance spectrum of PMC-2

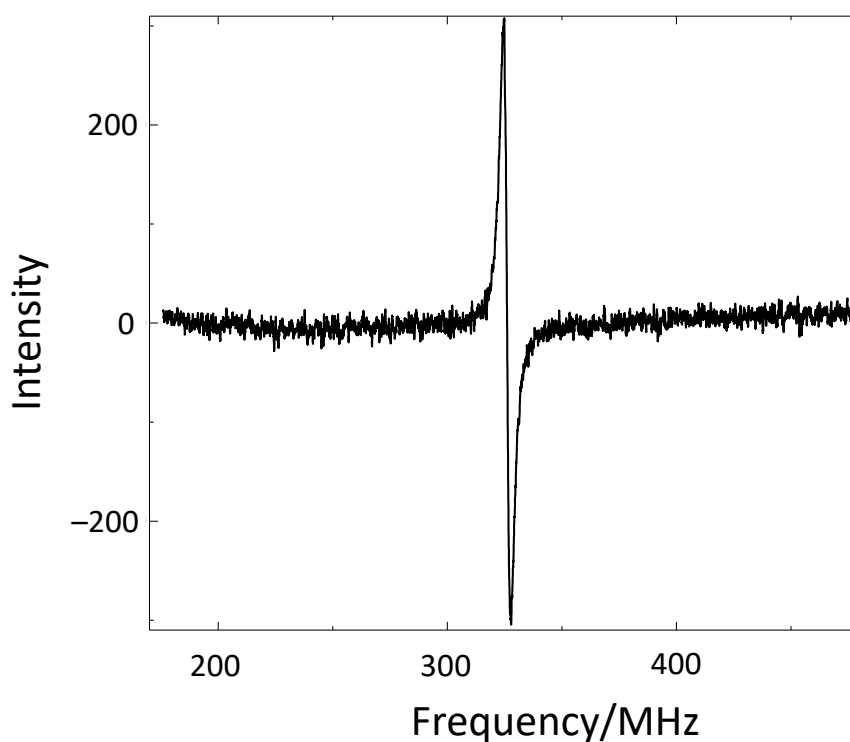


Fig. S6 Electron spin resonance spectrum of **PMC-2** at room temperature

Electron spin resonance (ESR) spectrum of **PMC-2** indicated that a sharp signal ( $g = 2.003$ ) was derived from the existence of  $\text{NDI}^{\cdot-}$  species. Although ICP analysis indicated that a half of NDI-py moieties were reduced, the amount of spins in **PMC-2** calculated from TEMPOL as a reference sample was corresponding to only 2% of NDI-py moieties. The reason for the decrease of the spin density is that most of the radical spins are inactive even at room temperature likely due to the coupling of radical spins caused by the random charge localization. The ESR signal of  $\text{Co}^{2+}$  ion was too broad to detect at room temperature.

## Direct current (DC) magnetic susceptibility of PMC-2

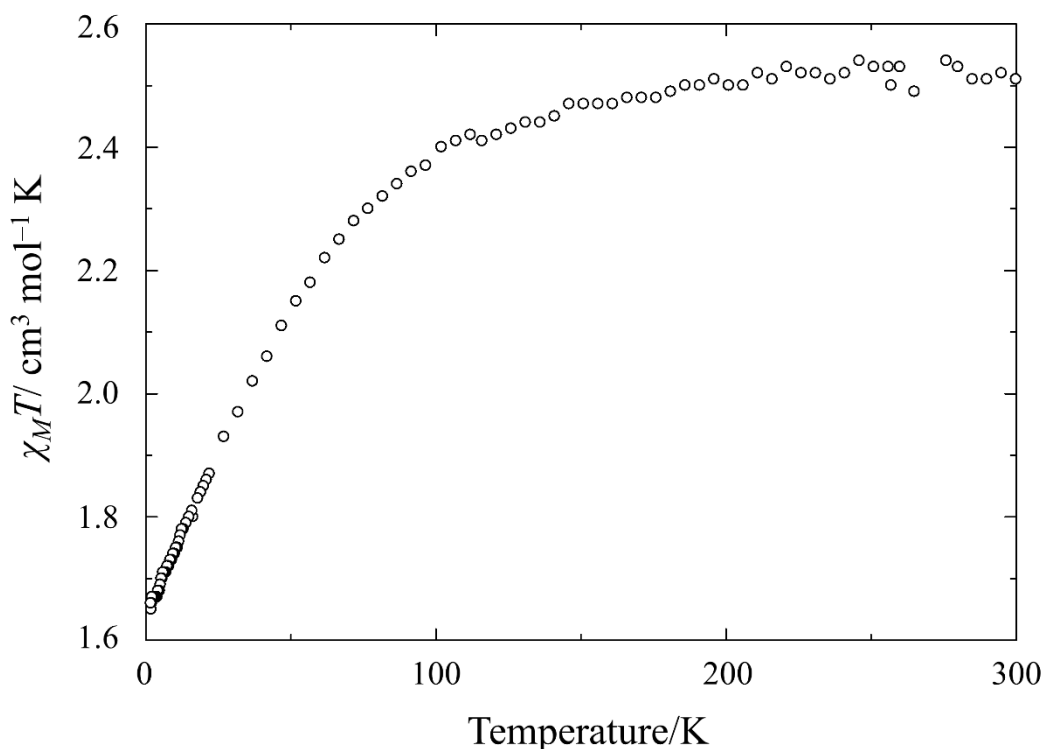


Fig. S7 Temperature-dependent DC magnetic susceptibility under 1000 Oe

Static magnetic property of **PMC-2** was measured in the range of 1.8–300 K. Temperature ( $T$ ) dependence of  $\chi_M T$ , where  $\chi_M$  is the molar magnetic susceptibility of **PMC-2** is presented in Fig. S7. As discussed in page S6, the percentage of reduced NDI-py moieties was only 2%. Thus, the estimated  $\chi_M T$  value derived from NDI-py radicals is  $0.0075 \text{ cm}^{-3} \text{ mol}^{-1} \text{ K}$  (2% of the theoretical  $\chi_M T$  value ( $0.375 \text{ cm}^{-3} \text{ mol}^{-1} \text{ K}$ ) for  $S = 1/2$  free spin). This value is negligible compared with the observed  $\chi_M T$  value in Fig. S7. Therefore, we considered that only  $\text{Co}^{2+}$  ion contributed to the magnetic susceptibility. The  $\chi_M T$  value at 300 K was  $2.51 \text{ cm}^3 \text{ mol}^{-1} \text{ K}$ . Since the calculated  $\chi_M T$  value of  $S = 3/2$  spin centre is  $1.875 \text{ cm}^{-3} \text{ mol}^{-1} \text{ K}$ , the increase of the  $\chi_M T$  value at 300 K can be explained by the significant contribution from orbital angular momentum of  $\text{Co}^{2+}$  ion. The  $\chi_M T$  value gradually decreased to  $1.65 \text{ cm}^3 \text{ mol}^{-1} \text{ K}$  at 1.8 K. There are two possible processes for this significant decreasing. One is the local zero-field splitting effects and the other is the antiferromagnetic dipole-dipole interactions between  $\text{Co}^{2+}$  ions. Since the distance between  $\text{Co}^{2+}$  ion is  $11.875 \text{ \AA}$ , the magnetic dipole-dipole interaction can be almost ignorable. Therefore, the decreasing of  $\chi_M T$  value in the lower temperature originates from the local zero-field splitting effects, which is typically observed in high-spin  $\text{Co}^{2+}$  ion.<sup>S6</sup>

## Thermogravimetry of PMC-2

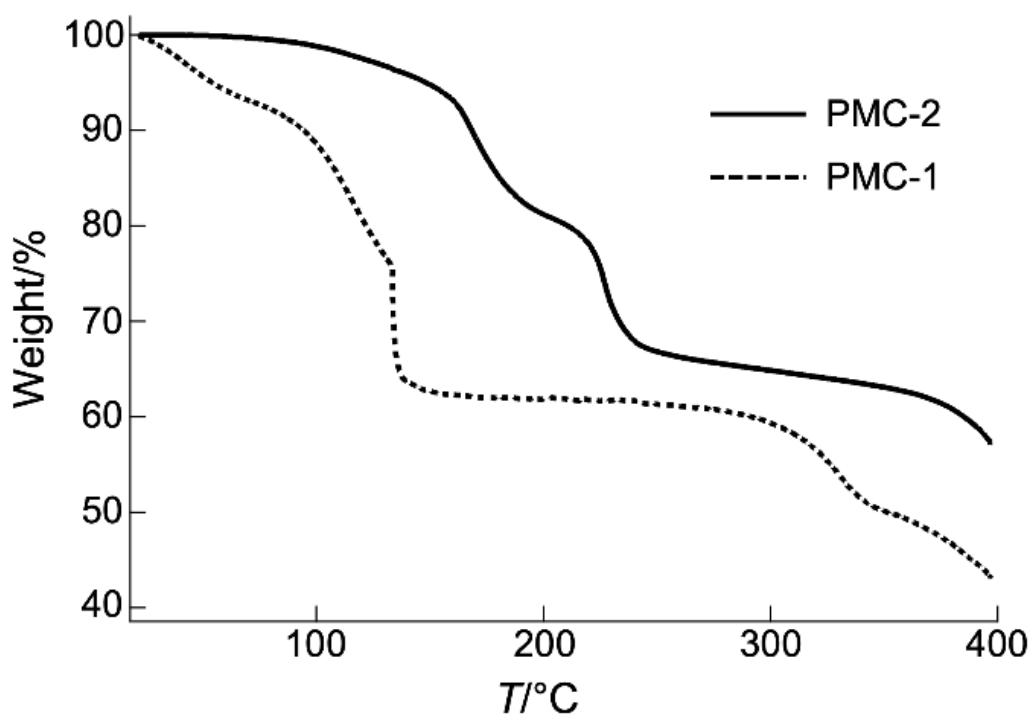


Fig. S8 Thermogravimetric analyses (TGA) of **PMC-2** (solid line) and **PMC-1** (broken line) at a heating rate of 5 °C /min.

### Weight loss of PMC-2 under N<sub>2</sub> gas flow

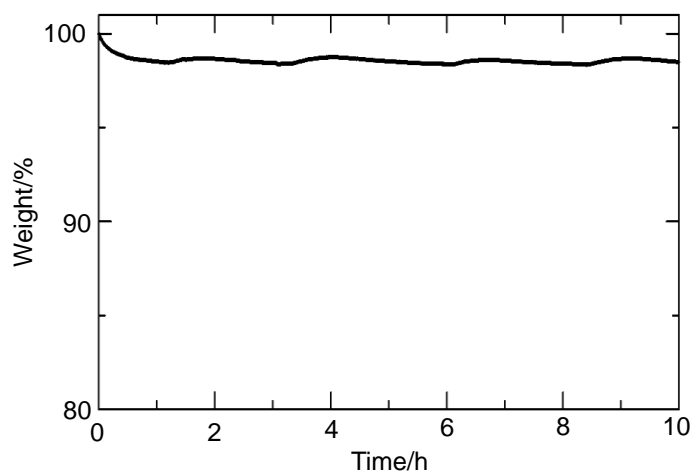


Fig. S9 Change of weight of **PMC-2** under N<sub>2</sub> gas flow (100 mL/min) at room temperature.

The initial weight loss is probably due to the evaporation of solvent adsorbed on the surface of crystals. The final weight after 10 hours is regarded as 100% weight in Fig. 2 in the manuscript.

### Time-dependent powder X-ray diffraction (PXRD) patterns of PMC-2

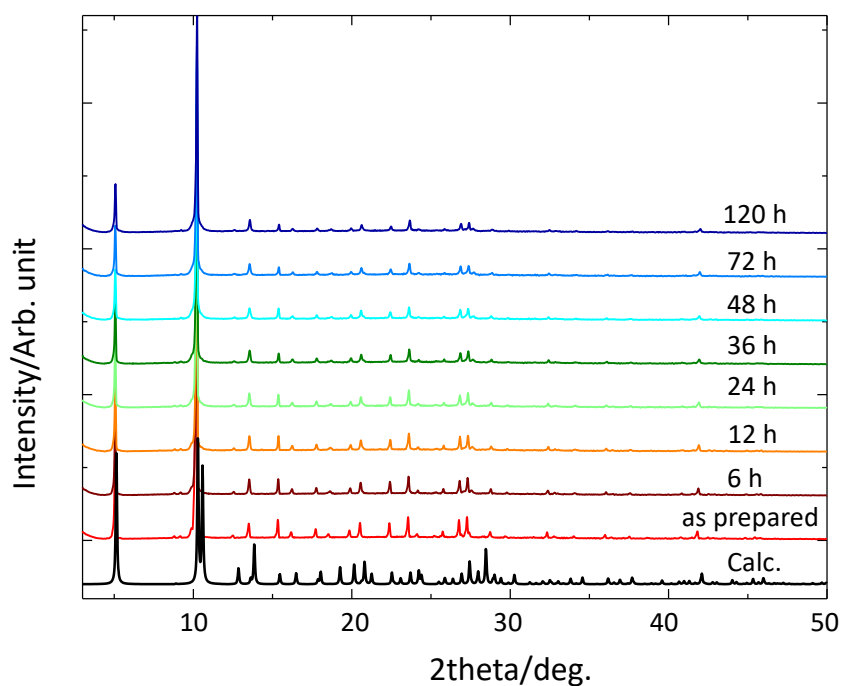


Fig. S10 Time-dependent PXRD patterns of **PMC-2** exposed to ambient air under the dark condition.

### Arrhenius plots of conductivities in PMC-2 and PMC-1

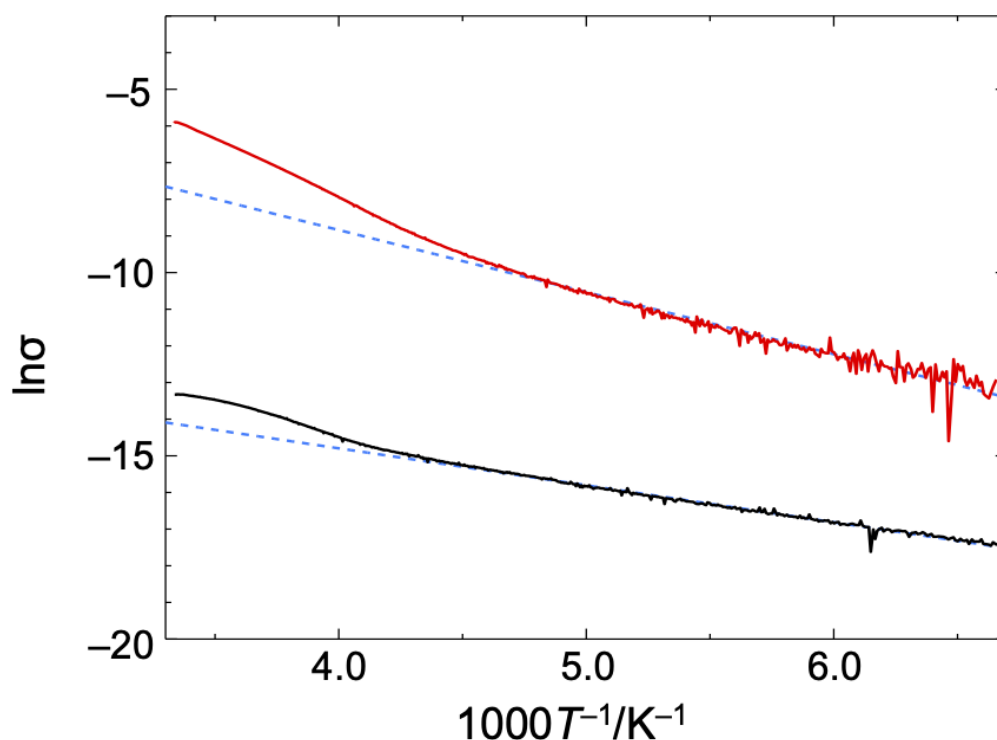


Fig. S11 Arrhenius plots of conductivities in **PMC-2** (black line) and **PMC-1** (red line)

Fitting the data in the range of 150–222 K for **PMC-2** and **PMC-1** with the Arrhenius equation  $\sigma = \sigma_0 \exp(E_a/kT)$ , where  $\sigma_0$  is the prefactor,  $E_a$  is the activation energy,  $k$  is the Boltzmann constant and  $T$  is the temperature, gives  $E_a$  of 82 meV and 145 meV for **PMC-2** and **PMC-1**, respectively.

### References

- [S1] G. M. Sheldrick, *Acta Cryst.* 2015, **A71**, 3.
- [S2] G. M. Sheldrick, *Acta Cryst.* 2015, **C71**, 3.
- [S3] Yadokari-XG, Software for Crystal Structure Analyses, K. Wakita (2001); Release of Software (Yadokari-XG 2009) for Crystal Structure Analyses, C. Kabuto, S. Akine, T. Nemoto, E. Kwon, *J. Cryst. Soc. Jpn.* 2009, **51**, 218–224.
- [S4] O. V. Dolomanov, L. J. Bourhis, R. J. Gildea, J. A. K. Howard, and H. Puschmann, *J. Appl. Cryst.*, 2009, **42**, 339–341.
- [S5] H. Iguchi, A. Nafady, S. Takaishi, M. Yamashita, A. M. Bond, *Inorg. Chem.*, 2014, **53**, 4022–4028.
- [S6] F. Lloret, M. Julve, J. Cano, R. Ruiz-García, E. Pardo, *Inorg. Chim. Acta.*, 2008, **361**, 3432–3445.